

Desorption of physisorbed molecular oxygen from coronene films and graphite surfaces

Cite as: J. Chem. Phys. **156**, 194307 (2022); <https://doi.org/10.1063/5.0087870>

Submitted: 10 February 2022 • Accepted: 14 April 2022 • Accepted Manuscript Online: 15 April 2022 • Published Online: 19 May 2022

 Abdi Salam Mohamed Ibrahim,  Sabine Morisset,  Saoud Baouche, et al.



View Online



Export Citation



CrossMark

ARTICLES YOU MAY BE INTERESTED IN

[Solution structures and ultrafast vibrational energy dissipation dynamics in cyclotetramethylene tetranitramine](#)

The Journal of Chemical Physics **156**, 194305 (2022); <https://doi.org/10.1063/5.0087297>

[A consistent and accurate ab initio parametrization of density functional dispersion correction \(DFT-D\) for the 94 elements H-Pu](#)

The Journal of Chemical Physics **132**, 154104 (2010); <https://doi.org/10.1063/1.3382344>

[Chemical physics software](#)

The Journal of Chemical Physics **155**, 010401 (2021); <https://doi.org/10.1063/5.0059886>

Lock-in Amplifiers
up to 600 MHz



Zurich
Instruments



Desorption of physisorbed molecular oxygen from coronene films and graphite surfaces

Cite as: J. Chem. Phys. 156, 194307 (2022); doi: 10.1063/5.0087870

Submitted: 10 February 2022 • Accepted: 14 April 2022 •

Published Online: 19 May 2022



View Online



Export Citation



CrossMark

Abdi Salam Mohamed Ibrahim,^{1,a)} Sabine Morisset,² Saoud Baouche,¹ and Francois Dulieu^{1,a)}

AFFILIATIONS

¹CY Cergy Paris Université, Sorbonne Université, Observatoire de Paris, PSL Université, CNRS, LERMA, F-95000 Cergy-Pontoise, France

²Institut des Sciences Moléculaires d'Orsay, ISMO, CNRS, Université Paris-Sud, Université Paris Saclay, F-91405 Orsay, France

^{a)}Authors to whom correspondence should be addressed: abdi-salam.mohamed-ibrahim@cyu.fr and francois.dulieu@cyu.fr

ABSTRACT

We present a study on the adsorption and desorption of molecular oxygen (O_2) on highly oriented pyrolytic graphite and coronene films deposited on it. To this end, density functional theory calculations were performed and experiments were made using the FORMOLISM device, which combines ultra-high vacuum, cryogenics, atomic or molecular beams, and mass spectrometry techniques. We first studied the desorption kinetics of dioxygen (O_2) on a coronene film and graphite at 15 K using the thermally programmed desorption technique. We observed that the desorption of O_2 occurs at a lower temperature on coronene than on graphite. We deduce the binding energies that are 12.5 kJ/mol on graphite and 10.6 kJ/mol on coronene films (pre-exponential factor, $6.88 \times 10^{14} \text{ s}^{-1}$). The graphite surfaces partially covered with coronene show both adsorption energies. In combination with theoretical density function theory (DFT) calculations using graphene and coronene as surfaces, we observe that the experimental results are in good agreement with the theoretical calculations. For the adsorption of the O_2 molecule, two orientations are possible: parallel or perpendicular to the surface. It seems that O_2 is best bound parallel to the surface and has a preference for the internal sites of the coronene.

Published under an exclusive license by AIP Publishing. <https://doi.org/10.1063/5.0087870>

I. INTRODUCTION

The discovery of several carbon allotropes (graphene, fullerene, and carbon nanotubes) in recent years has made these elements some of the most studied at the moment by the scientific community. Carbon-based nanomaterials possess outstanding physico-chemical properties, such as high thermal and electrical stability, corrosion resistance, and good thermal conduction. Thanks to these unique properties, carbon nanomaterials are used in various fields. However, as these materials usually consist of one or more atomic layers, their properties are extremely sensitive to environmental disturbances. Previous studies have suggested that exposure to gases, for example, has significant effects on their electrical and optical properties.¹⁻³ Among the adsorbates, oxygen (O_2) is one of the most important because it not only does alter the properties significantly through doping but is also the second most abundant gas in the atmosphere and is therefore very likely to affect the performance of materials.^{1,4} The interaction of O_2 with graphite has been extensively studied by various techniques.⁵⁻⁷

Experimental studies conducted using the thermally programmed desorption (TPD) technique have shown that molecular oxygen is physisorbed on graphite with an activation energy of 12 kJ/mol.⁷ Similarly, the photoemission spectra of the core levels also show no chemical changes or signs of charge transfer from O_2 to graphite.⁸ On the theoretical aspects, functional calculations of gradient-corrected density and spin polarization showed the absence of any type of charge transfer between O_2 and graphite.^{9,10} These studies suggest that the dominant interaction of molecular oxygen with carbon is of the van der Waals type and does not result in significant charge transfer for weakly adsorbed oxygen. The reason for this non-reactivity is the energy imbalance of a few tenths of eV between the unoccupied states of O_2 and the valence band of graphite. Therefore, a transformation of the unoccupied oxygen state is necessary for any reaction between the oxygen and the graphite surface to occur. It has been proven that a kinetic barrier prevents any lowering of oxygen states if the oxygen molecules are physisorbed at defect sites, such as gaps, folds, and edge planes.¹¹⁻¹³

The typical desorption temperature of O_2 on graphite is less than 45 K in the context of the laboratory. These temperature ranges do not have many terrestrial applications, but in the various interstellar or circumstellar environments, these temperatures are frequently encountered. In space, carbon also takes different forms, such as diamond, graphite, polycyclic aromatic hydrocarbons (PAHs), and amorphous carbons. Diamond and graphite are the two crystalline forms of carbon. Graphite is composed of an infinite number of aromatic planes parallel to each other. PAHs are a family of molecules composed of at least two aromatic rings to which hydrogen atoms are linked. They constitute a reservoir of carbon representing about 10% of the galactic carbon budget¹⁴ and represent the largest geometric area of the grain distribution.^{15–17} As such, they can participate in the depletion of the gas phase by sticking species on their cold surface very efficiently cooled by radiative transfer. The accretion of gaseous species is also accompanied by catalysis on the surfaces.¹⁸ In the case of O_2 , it is transformed into water by the very abundant hydrogen atoms.^{19–21} The accretion also corresponds to a depletion of the gaseous matter more easily observed and, once disappeared from direct observation, remains an enigma for astrochemistry. It is therefore important to know the desorption energies of species from PAHs, such as coronene and its archetype.

In this paper, we continue with the theme of the interaction of O_2 with carbon allotropes, and we will focus on the interaction of O_2 with coronene as a representative of polycyclic aromatic hydrocarbons (PAHs). There are two previous experimental studies closely related to our work: one is the study of the adsorption of PAHs on graphite^{22,23} and the other is the adsorption of O_2 on graphite.^{7,13} However, no attention was paid to the adsorption of O_2 on the PAHs. Here, we will study the adsorption of molecular oxygen on these two substrates (graphite and PAH) using the temperature programmed desorption (TPD) technique and compare them to quantum calculations.

II. EXPERIMENTAL METHODS

The experiments were carried out using the FORMOLISM Ultra-High Vacuum (UHV) setup with a base pressure lower than 1×10^{-10} mbar. This device is briefly described here, and more details

can be found in Ref. 24. The sample holder consists of a 1 cm diameter copper block mounted on a cryostat, covered with highly oriented pyrolytic graphite (HOPG, ZYA grade). A thermal switch is installed between the copper block and the cryostat. The sample temperature can be controlled between 10 and 780 K by means of a resistive heater that counterbalances the cooling power of the cryostat. HOPG has been cleaved several times using the “stripping tape” method at room temperature. This gives a surface made of several large terraces (micrometer scale) that contains limited defects and stepped edges. HOPG was cleaved in air immediately before being inserted into the vacuum chamber. It was mounted directly on the copper block using silver glue that resists high temperatures. Then, it was degassed by repeated heating cycles and annealing at $T_{max} = 750$ K. Previous studies reported that a HOPG heat treatment at greater than 700 K can clean the surface in UHV experiments.^{25–27}

A retractable crucible is installed on the UHV chamber. It is used to deposit the coronene ($\geq 99\%$ purity, Sigma-Aldrich) on the surface. The crucible is heated to 420 K to obtain a gentle evaporation of the coronene. A mobile screen can intercept the effusive beam of coronene and allows precise control of the deposition time. The crucible is thus positioned at 2 cm away from the HOPG surface. Between the deposits, the crucible is retracted into its own vacuum chamber to maintain a low background pressure in the sample chamber. Thus, a minimum of coronene molecules pollutes our main chamber, and the partial pressure of coronene remains very low. For the following, when we refer to the coronene surface, it is a coronene film deposited on the graphite.

The molecular oxygen is sent to the surface through a collimated molecular beam. Thanks to the three stages of differential pumping, the increase in the pressure in the main chamber is not detectable when the sample is cold. The O_2 flux is 3.3×10^{12} (mol/cm²)/s. When depositing O_2 on graphite (or coronene), the surface is maintained at 15 K. After deposition, the quadrupole mass spectrometer (QMS) is lowered and positioned 5 mm directly in front of the surface in order to proceed with Temperature Programmed Desorption (TPD). The surface is heated from 15 K to 60 K, with a constant heating ramp $\beta = 0.2$ K/s for all experiments. For the following, the temperature always refers to the surface temperature.

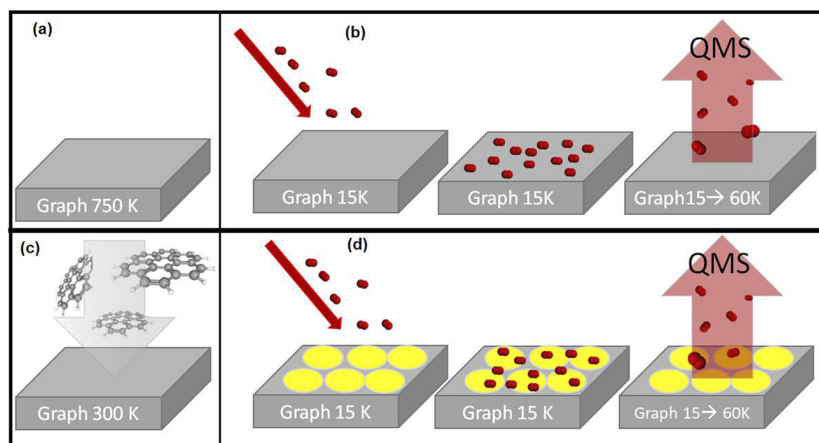


FIG. 1. Schematic representation of our experiments. Top: O_2 /HOPG experiment: (a) annealing of HOPG at 750 K and (b) O_2 deposited on HOPG at low temperature (15 K); after the deposition, a TPD of O_2 /HOPG is performed from 15 to 300 K. Bottom: O_2 on the $C_{24}H_{12}$ experiment: (c) $C_{24}H_{12}$ deposited on HOPG at room temperature and (d) deposition of O_2 on $C_{24}H_{12}$ at low temperature; after the deposition, a TPD of O_2 / $C_{24}H_{12}$ is performed from 15 to 60 K and O_2 molecules are completely desorbed from the coronene film. The red and yellow spheres are the O_2 and $C_{24}H_{12}$ molecules, respectively.

Figure 1 illustrates the sequence of the experiments. After annealing at 750 K the graphite substrate, the coronene film is deposited on the HOPG surface held at 280 K. The sample is cooled to 15 K, and a variable amount of O₂ is deposited. The TPD profiles of O₂ are recorded up to 60 K. The same coronene film can be used several times, and the temperature never rises above 200 K. There is no evidence of any chemical activity (reaction) between O₂ and the coronene film. The same amount of O₂ is desorbed from coronene or the graphite surface, indicating a similar sticking coefficient and no chemical loss. The coronene film is completely desorbed above 500 K.²⁸

III. EXPERIMENTAL RESULTS

A. O₂ adsorbed on the graphite surface

Figure 2 shows the desorption curves of O₂ as measured by the QMS signal for several exposure doses (0.44 ML, 0.86 ML, 1.7 ML, 4.4 ML, 7.3 ML, and 11.5 ML) of molecular oxygen deposited on the graphite at 15 K. Two desorption peaks are observed at about 42 and 30 K, which we call A_G and B, respectively. At low exposure, desorption shows that only peak A_G is present, centered around 42 K. This TPD peak is attributed to the strong interaction of O₂ molecules with graphite. The molecules occupy the most favorable adsorption sites in terms of energy and are closely bound to the graphite surface, desorbing late from the surface at temperatures up to 42 K. We therefore attribute this desorption peak A_G to the sub-monolayer regime. As exposure increases, a second characteristic peak, called the B peak, begins to appear at lower temperatures, centered around 30 K. Molecular oxygen is forced to gradually populate the less bound sites of the graphite, and/or to start a new layer, or at least to interact with other oxygen molecules already present on the surface.

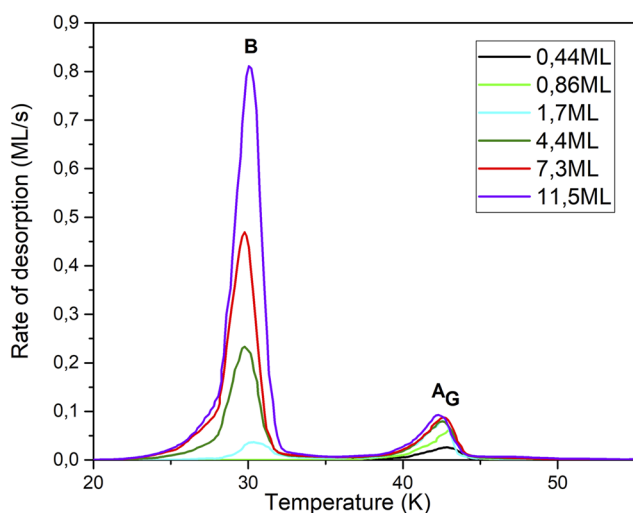


FIG. 2. TPD profiles of O₂ desorbing from highly oriented pyrolytic graphite with a heating rate of 0.2 K s⁻¹ for different doses. A_G refers to the sub-monolayer desorption from graphite, whereas B refers to the second/multilayer desorption peak.

If the exposure of O₂ is further increased (7.7–11.5 ML), we observe that the leading edge of the TPD curves stops moving to lower temperatures, which means that all adsorption sites seem equivalent, and any new incoming molecule is adsorbed on the first layers of molecules already adsorbed on the surface. In this case, the TPD curves show a desorption of order 0, and the maxima of the desorption peaks increase and start to move to higher temperatures with increasing doses. Our results are consistent with those of Ref. 7 that observed the desorption of O₂ on HOPG grade ZYB graphite (lower grade).

B. O₂ desorbing from coronene films

Since coronene molecules adsorb parallel to the graphite surface, it is possible to make a film made of a single layer of coronene.²² Following the work by Thrower *et al.*,²⁸ we obtain this complete layer by depositing slightly more coronene than required and make the excess desorb by annealing at around 350 K. Later, we will build a partial layer by exposing only half of the required time to obtain a complete layer.

Figure 3(a) shows the molecular oxygen desorption curve on a coronene film (1 ML) at 15 K.

It is to be noted that the O₂ exposures on coronene have been made under identical conditions to those of the deposits on graphite whose TPD is also shown in Fig. 3(b). For the coronene film, we also observe the two desorption peaks (A and B) previously reported in the case of O₂ on graphite, but this time, we find that the desorption of O₂ on the coronene desorbs between 32 and 38 K, which are lower temperatures than those observed for the graphite surface desorption. It can be seen that O₂ sublimates earlier on the coronene film than on the graphite. We conclude that the molecular oxygen adsorption sites are less bound on the coronene film than on the graphite, and we must keep this in mind as we will discuss it in Sec. IV when we analyze the interaction energies between this molecule and the substrate.

The green curves in Fig. 4 represent the TPDs of O₂ on the graphite partially covered with coronene. For comparison, these curves are superimposed on the TPD spectrum for the desorption of O₂ on the graphite fully covered with coronene (the blue curve) and the one on the graphite (the red curve) at 15 K. Focusing on the green curve, we observe three desorption peaks in three distinguished regions corresponding to B, A_C, and A_G, respectively.

In region B, between 24 and 32 K, measurements indicate that no significant change was observed at very low temperatures at the desorption of O₂ compared to the other two curves. On the other hand, for temperatures above 32 K in the A_C regions, we observe that there is a clear reduction in the contribution of O₂ desorbing from the coronene. The area of the green curve represents about two thirds of the blue desorption curve of O₂ on graphite completely covered by a layer of coronene. This missing third desorbs later from the graphite surface at the A_G peak. This indicates that the adsorbed O₂ is distributed between the coronene and the graphite and is likely to diffuse from the coronene surface to the graphite substrate and vice versa. This diffusion can occur during the heating phase of the sample where the molecules prefer to occupy the more energetic sites. Similarly, even if one increases the exposure of O₂ on this mixed surface, this does not lead to a noticeable saturation on the surface. We note that in this experiment, the molecular oxygen adsorption sites

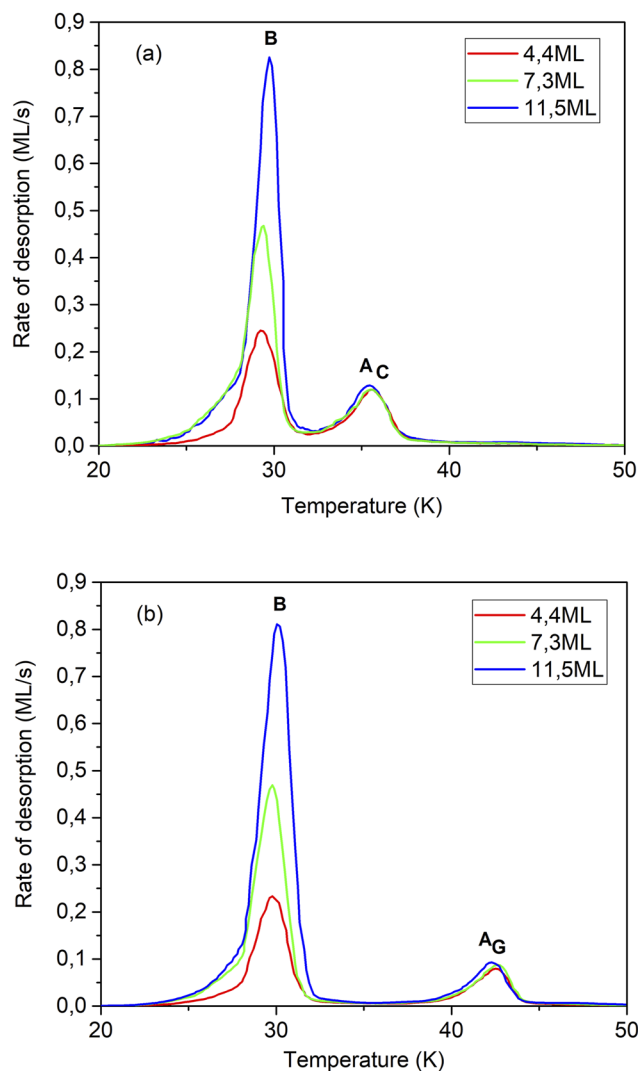


FIG. 3. (a) TPD of O₂ desorbing from a complete coronene film. The different exposure times to O₂ are shown in the legend. (b) Same experiment on graphite. A_G refers to the sub-monolayer desorption from graphite, and A_C to the sub-monolayer desorption from a coronene film, whereas B refers to the second/multilayer desorption peak.

are less strongly bound on the coronene film than on the graphite and that, on the other hand, this method allows us to diagnose sensitively the formation of the complete monolayer of coronene on the graphite, and validates, by another method, our previous calibration. Finally, we note that TPD peaks are well separated and do not exhibit broad features as, for example, always seen with physisorbed adsorbates on water ice substrates, even crystalline ones.^{29–31} Despite the fact that there should be steps due to the non-continuity of the coronene film on the graphite, we do not detect them, so we conclude that they are not favorable adsorption sites, and therefore, they should have a binding energy lower than the multilayer binding energy.

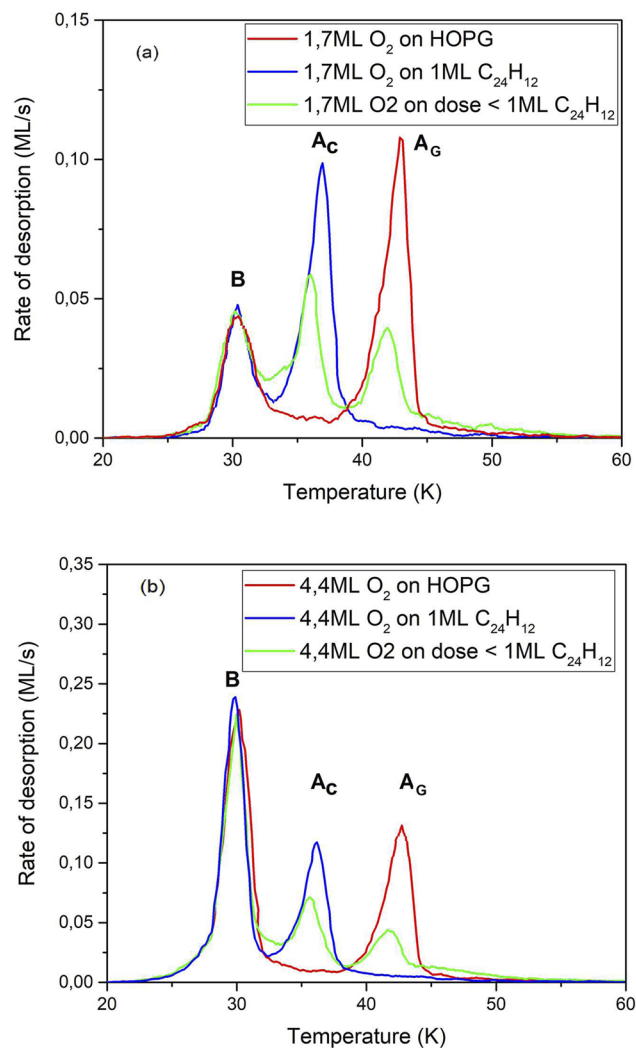


FIG. 4. TPD spectra of O₂ desorbing from different substrates: HOPG (red curve), complete coronene film (blue curve), and partial coverage of the coronene film on graphite (green curve): (a) 1.7 ML of O₂ and (b) 4.4 ML of O₂.

IV. THEORETICAL CALCULATIONS

In this section, the interaction between a graphenic surface and the O₂ molecule and between an O₂ molecule and a coronene deposited on a graphenic surface are calculated by Density Functional Theory (DFT) using the Quantum Espresso package.^{32,33} The van der Waals functional (vdW)^{34–38} is used for the description of the exchange–correlation terms. Ultra-soft pseudopotentials are used. The kinetic energy cutoff is 50 Ry for the wave function and 350 Ry for the charge density. The basis functions in DFT codes can be a Gaussian³⁹ or planewave^{32,33} basis set. In the Quantum Espresso code,^{32,33} the basis functions are planewaves. In Gaussian DFT, the basis functions are local atomic orbitals. Only localized orbital approaches have problem with the basis set superposition

errors (BSSE)^{39,40} in DFT calculations; therefore, we should avoid this problem in the present study.

For the interaction between the coronene and the graphenic surface, the vdW-DF-CX³⁵ functional has been used. The DFT calculations are carried out for a 7×7 graphene supercell, including 98 carbon atoms for the graphenic surface and 36 atoms for the coronene ($C_{24}H_{12}$) and 2 oxygen atoms for the dioxygen molecule using 4×4 k-points. As seen in a previous paper,⁴¹ the vdW-DF-CX functional allows obtaining interaction energy between the coronene and the graphenic surface of -1.74 eV at a large distance of 3.24 Å, in good agreement with the results reported in the study by Throter *et al.*^{22,43} This equilibrium geometry is obtained for an AB stacking^{22,41} as seen on the right part of Fig. 5.

For the interaction between the graphene surface and the O_2 molecule, the vdW-DF-CX functional³⁵ has also been used to compare with our previous calculations (O_2 on coronene on the graphene surface) and to take into account the physisorption of the O_2 molecule at a large distance. The DFT calculations are carried out on a 3×3 graphene supercell, including 18 carbon atoms for the graphene surface and 2 atoms for the dioxygen molecule using 6×6 k-points.

For the O_2 /graphene system and for O_2 on coronene deposited on the graphene surface, the interaction energy is calculated as follows:

$$\Delta E_{int} = E_{O_2/surface} - \epsilon E_{coronene} - E_{O_2}, \quad (1)$$

where E_{O_2} is the energy of the isolated O_2 molecule, $E_{coronene}$ is the energy isolated coronene molecule, and ϵ is 1 in the case of O_2 on coronene deposited on the graphene surface and 0 in the case of the O_2 /graphene system.

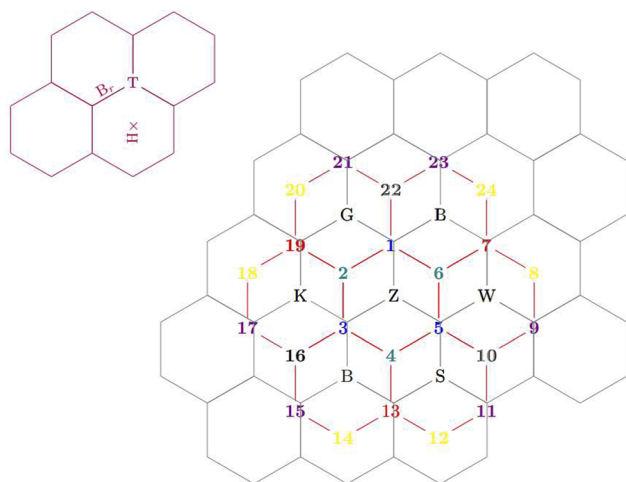


FIG. 5. Left (in purple): adsorption sites for the O_2 molecule on the graphenic surface: top site (T) above the carbon atom, bridge site (B_r) between two carbon atoms, and hollow site (H) in the center of the hexagon. Right: coronene deposited on the graphenic surface. Red and black: inner edge sites above the top (red) or hollow (black) site of the graphite. Yellow and purple: outer edge sites above the top (yellow) or hollow (purple) site of the graphite. Teal and blue: center sites above the top (teal) or hollow (blue) sites of the graphite. Letters indicate the bare top site of the graphenic surface.

TABLE I. Interaction energy of O_2 with the graphenic surface as a function of the orientation of the dioxygen molecule and the adsorption site.

O_2 orientation	Site (Fig. 5)	ΔE_{int} (kJ/mol)
Parallel	T	-14.964
Parallel	B_r	-13.758
Parallel	H	-13.720
Perpendicular	B_r	-11.597
Perpendicular	T	-11.529
Perpendicular	H	-12.205

For the adsorption of the O_2 molecule, two orientations are possible: parallel or perpendicular to the surface. On the graphenic surface, we have tested several adsorption sites: top site above a carbon atom, bridge site between two carbon atoms, and hollow site in the center of the hexagon, as seen on the top left part of Fig. 5. In Table I, the adsorption energies of the O_2 molecule on a graphenic surface as a function of the orientation of O_2 parallel and perpendicular to the surface for each adsorption site are reported. The most stable molecule is obtained for the parallel orientation in the top site (~ -15.0 kJ/mol), whereas hollow and bridge sites have slightly lower binding energies (~ -13.7 – 8 kJ/mol) also for the parallel orientation, which is, as intuition expects, the more favorable orientation. In these calculations, the distance on the graphite surface is higher than 3 Å whatever the adsorption site.

The coronene is adsorbed on the graphene surface in AB stacking. Several coronene sites are identified: outer edges sites (15, 17, 21, 23, 9, and 11 in Fig. 5), inner edges sites (19, 13, and 7 in Fig. 5), and center sites (1, 3, and 5 in Fig. 5) above a top site of the graphite; outer edge sites (20, 24, 8, 12, 14, and 18 in Fig. 5), inner edge sites (16, 10, and 22 in Fig. 5), and center sites (2, 4, and 6 in Fig. 5) above a hollow site of the graphene surface. In Table II, the adsorption energies as a function of the orientation of the O_2 molecule and for different sites of the coronene are reported. The most stable of O_2 molecule adsorption are also obtained for the parallel orientations. For one coronene site, the adsorption of O_2 is not influenced by the site hollow or top of the graphenic surface. The most

TABLE II. Interaction energy of O_2 with the coronene deposited on the graphenic surface as a function of the orientation of the dioxygen molecule and the adsorption sites.

Orientation	Site (Fig. 5)	ΔE_{int} (kJ/mol)
Parallel	2	-13.1509
Parallel	3	-13.0930
Parallel	18	-10.4204
Parallel	17	-10.5072
Parallel	16	-11.7036
Parallel	19	-10.8546
Perpendicular	2	-9.8125
Perpendicular	3	-9.5231
Perpendicular	18	-6.8601
Perpendicular	19	-8.3652
Perpendicular	21	-6.3680

stable O₂ molecule adsorption is obtained for the center site of the coronene whatever the hollow or top site of the graphenic surface. As seen on the graphene surface, the physisorption distance of O₂ on the coronene deposited on the graphenic surface is also higher than 3 Å whatever the adsorption site.

V. DISCUSSION

In order to describe the desorption kinetics, it is necessary to determine the surface coverage in terms of the number of adsorbed monolayers (ML) that result from a given exposure to the gas of interest. To determine the coverage for a given TPD trace, we note that the mass spectrometer signal for a desorbing species is directly proportional to its desorption rate. The TPD O₂ spectra on HOPG are thus analyzed using simple Arrhenius kinetics of the type,^{31,43,44}

$$r(T) = -\frac{dN}{dT} = AN^n \exp\left(-\frac{E_{des}}{k_B T}\right), \quad (2)$$

where $r(T)$ is the desorption rate (molecule cm⁻² s⁻¹), N is the number density of molecules adsorbed on the surface (molecule cm⁻² s⁻¹), n is the order of the desorption kinetics and corresponds to the stoichiometric coefficients, i.e., the number of reagents necessary to activate the desorption reactions, and is equal to 1 in our case. A is the pre-exponential factor (s⁻¹), $k_B = 1.38 \times 10^{-23}$ J K⁻¹ is the Boltzmann constant, T is the temperature of the surface (K), and E_{des} is the activation energy for desorption (J). We remind a useful conversion of energy units (1 kJ mol⁻¹ = 120 K/k_B).

We can invert the equation and obtain

$$E_{des} = k_B T \ln\left(\frac{AN(T)}{r(T)}\right). \quad (3)$$

To calculate the desorption energy E_{des} , Eq. (2) is solved using an experimental TPD spectrum with different coverages. We thus took $A = 6.88 \times 10^{14}$ s⁻¹ following the method proposed in Refs. 45 and 46.

Using this pre-exponential factor, we calculate the binding energy of molecular oxygen adsorbed on graphite, which is 12.5 kJ/mol. Our value is in good agreement with the value estimated by Ulbricht,¹³ which was 12 kJ/mol for a pre-exponential factor of $A = 6.88 \times 10^{14}$ s⁻¹. Using Eq. (7) of Ref. 47 made to compare two couples of binding energies and pre-exponential factors, we conclude that the matching is excellent.

In the same way, we study the desorption energy of O₂ on the coronene (deposited on the graphite) using also the same method of inversion of the equation of Polanyi–Wigner. We find that the desorption energy of the O₂ of the coronene is equal to 10.6 kJ/mol ($A = 6.88 \times 10^{14}$ s⁻¹). The comparison of these desorption energies shows that O₂ is more strongly bound to graphite than to the coronene film, as expected. We note a difference in the desorption energy of -1.9 kJ/mol between the coronene film and graphite. The value of the binding energy of the O₂ multilayer will be useful later. The measurement has been reported many times (see Table 2 in Ref. 31). Using the pre-exponential factor of 6.88×10^{14} s⁻¹, it gives a binding energy of 9.1 kJ/mol. Adsorption sites with lower binding energies will not be detectable in TPD experiments.

In Tables I and II, we have summarized the O₂ adsorption energies on graphite and coronene obtained from theoretical calculations. For O₂ interacting with a graphite surface, the most stable adsorption energy (minimum energy) is for the molecule parallel to the surface with an energy ≈14 kJ/mol, and this energy varies slightly with the position of the molecule on the surface, which has very little or no corrugation. For O₂ on coronene adsorbed on a graphite surface, we notice that the adsorption energy of the O₂ molecule parallel to the coronene is lower than for the molecule perpendicular to the coronene surface, like in the simpler case of adsorption on graphite. Therefore, the orientation of the O₂ molecule is probably not the origin of the difference in desorption energy measured, as the effect is about the same on the two substrates and that each time the parallel configuration is found to be more stable.

The position of the molecule is more sensitive. O₂ is more bound when it adsorbs at the center of the coronene (sites 2 and 3) than at the edges of the coronene (sites 16, 17, 18, 19, and 21), and the adsorption energy varies from 13.15 kJ/mol to 10.42 kJ/mol (parallel O₂) and 9.81 to 6.86 kJ/mol (perpendicular O₂). Therefore, the O₂ molecule on coronene adsorbed on a graphite surface, and little effect is observed depending on whether the adsorption site of the molecule on the coronene is on a top site of graphite or a hollow site of graphite. It is also found that the most stable equilibrium geometry (energy minimum) is 13.09 or 13.15 kJ/mol for parallel O₂ adsorbed on the deposited central ring of coronene and is 14.96–13.72 kJ/mol for O₂ on graphite.

We now compare experimental results where a single value of desorption energy for each substrate is found, with the multiple values of the adsorption energy calculated. It is difficult to compare static, state-by-state results from calculations with dynamical measurements and averaged results from experiments. The first remark is that globally we find that both the calculated binding energies and the measured desorption energies show that the interactions are weaker on the coronene film than on graphite. However, the experiments do not show distributions of energies, in particular when there is an incomplete film of coronene. In this case, the TPD curves are still well peaked and do not really exhibit broadened profiles. It is not a limitation of the technique as we could measure the distribution of binding energies for amorphous substrates.^{31,43}

The second remark to make is that the absolute calibration of the energies for the calculations is more uncertain than the relative deviations. Taking into account the possible discussion on the choice on the pre-exponential factor A , which, in turn, affects the determination of E_{des} , also for experiments, the difference in desorption energies is particularly meaningful. This is why we will pay specific attention to the difference of energy between the two surfaces. To push forward the comparison, we will now study 3 possible ways to make comparisons.

For the first scenario, we calculate the arithmetic average of the O₂ adsorption energies (parallel and perpendicular) on graphite and coronene from Tables I and II. We find 12.95 kJ/mol for the arithmetic average of O₂ on graphite and 10.06 kJ/mol for O₂ on coronene. For this hypothesis, we note that the O₂ adsorption energy values for these two surfaces are very close to the experimental values although the difference is certainly higher (almost 3 kJ/mol instead of 2).

For the second scenario, we are only interested in the parallel configuration because the perpendicular geometry is systematically less bounded than the parallel geometry, and some binding energies of the perpendicular geometry have values lower than the limit of the multilayer binding energy and therefore are not measurable. Of this effect, we believe that the O₂ configuration parallel to the surface is energetically more favorable to our experimental result. However, since we start to select the adsorption configuration, we also need to discuss if all sites will be equally populated. The case of the coronene film is the most complicated. For the adsorption of the O₂ molecule on the surface of the coronene, the molecule can choose the best adsorption sites on the center of the coronene ring (with $E = 13.09$ kJ/mol or 13.15 kJ/mol). However, this type of site is rare because there is a greater probability of adsorption on the sites located at the edges of the coronene, which are 6 times more numerous than the central cycle sites, as we can see in Fig. 5. The central ring of coronene has 6 adsorption sites; the teal sites (2; 4; 6) and blue sites (1; 3; 5) correspond to the adsorption energies of 13.15 and 13.09 kJ/mol, respectively. Similarly, the sites located on the edges present 18 adsorption sites (6 sites in yellow, 6 sites in purple, 3 sites in red, and 3 sites in black). These outer sites have an average binding energy of 10.73 kJ/mol. Finally, for the average of the parallel configuration, weighted by the number of adsorption sites, we find an adsorption energy that is equal to 11.29 kJ/mol. For graphite, the weighted arithmetic average of the parallel configuration gives 13.91 kJ/mol. Of course, these values are higher than for the arithmetic average since we have removed the perpendicular geometry cases that have a lower binding energy. This second scenario allows us to understand that in experiments, the signal is possibly dominated by the edge sites of coronene that present a lower adsorption energy; these sites do not benefit from the infinite and symmetrical surface character of graphite. We note that the difference is closer to what measured than in the first scenario.

The last scenario is the following: we agree that the parallel O₂ configuration is the most stable. We take the most stable value of O₂ on graphite and coronene, which is of 14.96 and 13.15 kJ/mol, respectively, and obtain a difference of 1.81 kJ/mol. If we compare these theoretical and experimental values, we see that the theoretical desorption energy is higher than the experimental value but has a good agreement for the difference.

In fact, none of the ways of comparing the static calculations and the dynamic result of the experiment is fully satisfactory even if each of these approaches makes it possible to highlight a particular point. Nevertheless, the difficult point to reconcile is the apparent single binding energy measured for both partial and complete coronene films, whereas calculations and common sense indicate that there are different adsorption sites and that one should therefore be able to measure a binding energy distribution, which is not the case. The coronene films, even incomplete, do not act as a topologically disordered surface, such as crystalline water, which exhibit binding energy distribution.⁴⁸ Despite the necessary present steps between two coronene molecules on incomplete films, this does not provide favorable adsorption sites. There would be no O₂ molecule adsorbing on the steps caused by the coronene boundary. Moreover, calculations are made with isolated molecules and fully neglect lateral interactions of adsorbates that should play an important role in experiments.

It is therefore possible that during sublimation, the oxygen molecules organize themselves into clusters of molecules above each coronene molecule. The O₂ molecules would also be organized in a “crown” around the central molecule above the central site. Thus, the apparent difference in the binding energy of coronene and graphite films would be the difference of the lowest adsorption site, and in both cases, lateral interactions would add geometrical constraints on other adsorbates, slightly reducing the effective binding energy of the O₂ film or cluster. Of course, all this remains speculative.

VI. CONCLUSION

We have studied the adsorption and desorption of O₂ from graphite or coronene films. The desorption peaks observed after the TPD of O₂ adsorbed on bare graphite or on a full or partial layer of coronene deposited on graphite are sharp and narrow and correspond to desorption energies of 12.5 and 10.6 kJ/mol (graphite and coronene, respectively; $A = 6.88 \times 10^{14} \text{ s}^{-1}$). Thus, the adsorption and desorption of O₂ can be used as a sensitive means of assessing the coverage of coronene on graphite since the two characteristic peaks are modulated in intensity as a function of coronene coverage.

Quantum calculations were performed, and it was found in all cases that O₂ has a higher binding energy when adsorbed parallel to the surface. The binding energy is greater for sites above the inner part of the coronene molecule. The graphite on which coronene is adsorbed has a very small influence on O₂ adsorption. Although the calculated binding energy values are slightly higher than the measured values, they are in good agreement and confirm that the O₂ adsorption sites on the edge or steps of the coronene adsorbed on graphite have a lower binding energy and so do not contribute to the desorption signal.

ACKNOWLEDGMENTS

This work was supported by the Programme National “Physique et Chimie du Milieu Interstellaire” (PCMI) of CNRS/INSU with INC/INP co-funded by CEA and CNES and by DIM-ACAV+, a funding program of the Region Ile de France. The authors thank Nathalie Rougeau and Stephanie Cazaux for fruitful discussions.

AUTHOR DECLARATIONS

Conflict of Interest

The authors have no conflicts to disclose.

DATA AVAILABILITY

The data that support the findings of this study are available from the corresponding authors upon reasonable request.

REFERENCES

- ¹H.-C. Chang, Y.-J. Huang, H.-Y. Chang, W.-J. Su, Y.-T. Shih, Y.-S. Huang, and K.-Y. Lee, “Oxygen adsorption effect on nitrogen-doped graphene electrical properties,” *Appl. Phys. Express* **7**(5), 055101 (2014).
- ²P. G. Collins, K. Bradley, M. Ishigami, and A. Zettl, “Extreme oxygen sensitivity of electronic properties of carbon nanotubes,” *Science* **287**(5459), 1801–1804 (2000).

- ³I. Santoso, R. S. Singh, P. K. Gogoi, T. C. Asmara, D. Wei, W. Chen, A. T. Wee, V. M. Pereira, and A. Rusydi, "Tunable optical absorption and interactions in graphene via oxygen plasma," *Phys. Rev. B* **89**(7), 075134 (2014).
- ⁴F. R. Bagan, A. Winchester, S. Ghosh, X. Zhang, L. Ma, M. Wang, H. Murakami, S. Talapatra, R. Vajtai, P. M. Ajayan *et al.*, "Adsorption energy of oxygen molecules on graphene and two-dimensional tungsten disulfide," *Sci. Rep.* **7**(1), 1774 (2017).
- ⁵M. Nielsen and J. P. McTague, "Oxygen monolayers adsorbed on graphite studied by neutron scattering," *Phys. Rev. B* **19**(6), 3096 (1979).
- ⁶M. F. Toney and S. C. Fain, "Low-energy electron diffraction study of molecular oxygen physisorbed on graphite," *Phys. Rev. B* **36**, 1248–1258 (1987).
- ⁷H. Ulbricht, G. Moos, and T. Hertel, "Physisorption of molecular oxygen on single-wall carbon nanotube bundles and graphite," *Phys. Rev. B* **66**, 075404 (2002).
- ⁸A. Nilsson, O. Björneholm, H. Tillborg, B. Herrnäs, R. J. Guest, A. Sandell, R. E. Palmer, and N. Mårtensson, "Core level spectroscopy of physisorbed molecules on graphite," *Surf. Sci.* **287–288**, 758–769 (1993) [Proceedings of the 8th International Conference on Solid Surfaces].
- ⁹P. Giannozzi, R. Car, and G. Scoles, "Oxygen adsorption on graphite and nanotubes," *J. Chem. Phys.* **118**(3), 1003–1006 (2003).
- ¹⁰D. C. Sorescu, K. D. Jordan, and P. Avouris, "Theoretical study of oxygen adsorption on graphite and the (8,0) single-walled carbon nanotube," *J. Phys. Chem. B* **105**(45), 11227–11232 (2001).
- ¹¹E. Castanier and C. Noguera, "Oxygen vacancies on MgO(100)," *Surf. Sci.* **364**(1), 1–16 (1996).
- ¹²G. Pacchioni, "Ab initio theory of point defects in oxide materials: Structure, properties, chemical reactivity," *Solid State Sci.* **2**(2), 161–179 (2000).
- ¹³H. Ulbricht, G. Moos, and T. Hertel, "Interaction of molecular oxygen with single-wall carbon nanotube bundles and graphite," *Surf. Sci.* **532–535**, 852–856 (2003) [Proceedings of the 7th International Conference on Nanometer-Scale Science and Technology and the 21st European Conference on Surface Science].
- ¹⁴A. G. G. M. Tielens, "The molecular universe," *Rev. Mod. Phys.* **85**, 1021–1081 (2013).
- ¹⁵F.-X. Desert, F. Boulanger, and J.-L. Puget, "Interstellar dust models for extinction and emission," *EDP Sciences* **237**, 215–236 (1990).
- ¹⁶B. T. Draine, "Interstellar dust models and evolutionary implications," [arXiv:0903.1658](https://arxiv.org/abs/0903.1658) (2009).
- ¹⁷J. C. Weingartner and B. T. Draine, "Dust grain-size distributions and extinction in the milky way, large magellanic cloud, and small magellanic cloud," *Astrophys. J.* **548**, 296–309 (2001).
- ¹⁸E. Rauls and L. Hornekaer, *Astrophys. J.* **679**, 531 (2008).
- ¹⁹H. M. Cuppen, S. Ioppolo, C. Romanzin, and H. Linnartz, "Water formation at low temperatures by surface O₂ hydrogenation II: The reaction network," *Phys. Chem. Chem. Phys.* **12**(38), 12077–12088 (2010).
- ²⁰F. Dulieu, L. Amiaud, E. Congiu, J.-H. Fillion, E. Matar, A. Momeni, V. Pirronello, and J. L. Lemaire, "Experimental evidence for water formation on interstellar dust grains by hydrogen and oxygen atoms," *Astron. Astrophys.* **512**, A30 (2010).
- ²¹N. Miyauchi, H. Hidaka, T. Chigai, A. Nagaoka, N. Watanabe, and A. Kouchi, "Formation of hydrogen peroxide and water from the reaction of cold hydrogen atoms with solid oxygen at 10K," *Chem. Phys. Lett.* **456**(1–3), 27–30 (2008).
- ²²J. D. Thrower, E. E. Friis, A. L. Skov, L. Nilsson, M. Andersen, L. Ferrighi, B. Jørgensen, S. Baouche, R. Balog, B. Hammer *et al.*, "Interaction between coronene and graphite from temperature-programmed desorption and DFT-*vdW* calculations: Importance of entropic effects and insights into graphite interlayer binding," *J. Phys. Chem. C* **117**(26), 13520–13529 (2013).
- ²³R. Zacharia, H. Ulbricht, and T. Hertel, "Interlayer cohesive energy of graphite from thermal desorption of polyaromatic hydrocarbons," *Phys. Rev. B* **69**(15), 155406 (2004).
- ²⁴E. Congiu, H. Chaabouni, C. Laffon, P. Parent, S. Baouche, and F. Dulieu, "Efficient surface formation route of interstellar hydroxylamine through NO hydrogenation. I. The submonolayer regime on interstellar relevant substrates," *J. Chem. Phys.* **137**(5), 054713 (2012).
- ²⁵D. V. Chakarov, L. Oesterlund, and B. Kasemo, "Water adsorption and coadsorption with potassium on graphite(0001)," *Langmuir* **11**(4), 1201–1214 (1995).
- ²⁶M. J. Dorko, T. R. Bryden, and S. J. Garrett, "Adsorption and photochemistry of CF₂Br₂ (halon 1202) on highly ordered pyrolytic graphite (HOPG)," *J. Phys. Chem. B* **104**(49), 11695–11703 (2000).
- ²⁷M. Z. Hossain, J. E. Johns, K. H. Bevan, H. J. Karmel, Y. T. Liang, S. Yoshimoto, K. Mukai, T. Koitaya, J. Yoshinobu, M. Kawai *et al.*, "Chemically homogeneous and thermally reversible oxidation of epitaxial graphene," *Nat. Chem.* **4**(4), 305 (2012).
- ²⁸J. D. Thrower, B. Jørgensen, E. E. Friis, S. Baouche, V. Mennella, A. C. Luntz, M. Andersen, B. Hammer, and L. Hornekaer, "Experimental evidence for the formation of highly superhydrogenated polycyclic aromatic hydrocarbons through H atom addition and their catalytic role in H₂ formation," *Astrophys. J.* **752**(1), 3 (2012).
- ²⁹G. a. Kimmel, K. P. Stevenson, Z. Dohnálek, R. S. Smith, and B. D. Kay, "Control of amorphous solid water morphology using molecular beams. I. Experimental results," *J. Chem. Phys.* **114**(12), 5284 (2001).
- ³⁰J. A. Noble, S. Diana, and F. Dulieu, "Segregation of O₂ and CO on the surface of dust grains determines the desorption energy of O₂," *Mon. Not. R. Astron. Soc.* **454**(3), 2636–2646 (2015).
- ³¹J. A. Noble, E. Congiu, F. Dulieu, and H. J. Fraser, "Thermal desorption characteristics of CO, O₂ and CO₂ on non-porous water, crystalline water and silicate surfaces at submonolayer and multilayer coverages," *Mon. Not. R. Astron. Soc.* **421**(1), 768–779 (2012).
- ³²P. Giannozzi, O. Andreussi, T. Brumme, O. Bunau, M. Buongiorno Nardelli, M. Calandra, R. Car, C. Cavazzoni, D. Ceresoli, M. Cococcioni, N. Colonna, I. Carnimeo, A. Dal Corso, S. de Gironcoli, P. Delugas, R. A. DiStasio, A. Ferretti, A. Floris, G. Fratesi, G. Fugallo, R. Gebauer, U. Gerstmann, F. Giustino, T. Gorni, J. Jia, M. Kawamura, H. Y. Ko, A. Kokalj, E. Küçükbenli, M. Lazzeri, M. Marsili, N. Marzari, F. Mauri, N. L. Nguyen, H. V. Nguyen, A. Otero-de-la-Roza, L. Paulatto, S. Poncè, D. Rocca, R. Sabatini, B. Santra, M. Schlipf, A. P. Seitsonen, A. Smogunov, I. Timrov, T. Thonhauser, P. Umari, N. Vast, X. Wu, and S. Baroni, "Advanced capabilities for materials modelling with quantum espresso," *J. Phys.: Condens. Matter* **29**, 465901 (2017).
- ³³P. Giannozzi, S. Baroni, N. Bonini, M. Calandra, R. Car, C. Cavazzoni, D. Ceresoli, G. L. Chiarotti, M. Cococcioni, I. Dabo, A. Dal Corso, S. de Gironcoli, S. Fabris, G. Fratesi, R. Gebauer, U. Gerstmann, C. Gougoussis, A. Kokalj, M. Lazzeri, L. Martin-Samos, N. Marzari, F. Mauri, R. Mazzarello, S. Paolini, A. Pasquarello, L. Paulatto, C. Sbraccia, S. Scandolo, G. Sclauzero, A. P. Seitsonen, A. Smogunov, P. Umari, and R. M. Wentzcovitch, "Quantum espresso: A modular and open-source software project for quantum simulations of materials," *J. Phys.: Condens. Matter* **21**, 395502 (2009).
- ³⁴K. Berland, V. R. Cooper, K. Lee, E. Schröder, T. Thonhauser, P. Hyldgaard, and B. I. Lundqvist, "Van der Waals forces in density functional theory: A review of the *vdW*-DF method," *Rep. Prog. Phys.* **78**, 066501 (2015).
- ³⁵K. Berland and P. Hyldgaard, "Exchange functional that tests the robustness of the plasmon description of the van der Waals density functional," *Phys. Rev. B* **89**, 035412 (2014).
- ³⁶D. C. Langreth, B. I. Lundqvist, S. D. Chakarova-Käck, V. R. Cooper, M. Dion, P. Hyldgaard, A. Kelkkanen, J. Kleis, L. Kong, S. Li, P. G. Moses, E. Murray, A. Puzder, H. Rydberg, E. Schröder, and T. Thonhauser, "A density functional for sparse matter," *J. Phys.: Condens. Matter* **21**, 084203 (2009).
- ³⁷K. Lee, E. Murray, L. Kong, B. Lundqvist, and D. C. Langreth, "Higher-accuracy van der Waals density functional," *Phys. Rev. B* **82**, 081101 (2010).
- ³⁸T. Thonhauser, V. R. Cooper, S. Li, A. Puzder, P. Hyldgaard, and D. C. Langreth, "Van der Waals density functional: Self-consistent potential and the nature of the van der Waals bond," *Phys. Rev. B* **76**, 125112 (2007).
- ³⁹J. G. Brandenburg, M. Alessio, B. Civalleri, M. F. Peintinger, T. Bredow, and S. Grimme, "Geometrical correction for the inter- and intramolecular basis set superposition error in periodic density functional theory calculations," *J. Phys. Chem. A* **117**, 9282–9292 (2013).
- ⁴⁰D. J. Carter and A. L. Rohl, "Benchmarking calculated lattice parameters and energies of molecular crystals using van der Waals functionals," *J. Chem. Theory Comput.* **10**, 3423–3437 (2014).
- ⁴¹S. Morisset, N. Rougeau, and D. Teillet-Billy, *Chem. Phys. Lett.* **679**, 225 (2017).
- ⁴²J. D. Thrower, E. E. Friis, A. L. Skov, B. Jørgensen, and L. Hornekaer, "Hydrogenation of PAH molecules through interaction with hydrogenated carbonaceous grains," *Phys. Chem. Chem. Phys.* **16**(8), 3381–3387 (2014).

⁴³L. Amiaud, "Interaction d'atomes et de molécules d'hydrogène avec des glaces d'eau à très basse température: Formation de H₂ dans le milieu interstellaire," Ph.D. thesis, Université de Cergy-Pontoise, 2006.

⁴⁴Z. Dohnálek, G. A. Kimmel, S. A. Joyce, P. Ayotte, R. S. Smith, and B. D. Kay, "Physisorption of CO on the MgO (100) surface," *J. Phys. Chem. B* **105**(18), 3747–3751 (2001).

⁴⁵M. Minissale, Y. Aikawa, E. Bergin, M. Bertin, W. Brown, S. Cazaux, S. Charnley, A. Coutens, H. Cuppen, V. Guzman, H. Linnartz, M. McCoustra, A. Rimola, J. G. M. Schrauwen, C. Toubin, P. Ugliengo, N. Watanabe, V. Wakelam, and F. Dulieu, "Thermal desorption of interstellar ices: A review on the controlling

parameters and their implications from snowlines to chemical complexity," *ACS Earth Space Chem.* **6**(3), 597–630 (2022).

⁴⁶S. L. Tait, Z. Dohnálek, C. T. Campbell, and B. D. Kay, "*n*-Alkanes on MgO(100). II. Chain length dependence of kinetic desorption parameters for small *n*-alkanes," *J. Chem. Phys.* **122**, 164708 (2005).

⁴⁷H. Chaabouni, S. Diana, T. Nguyen, and F. Dulieu, "Thermal desorption of formamide and methylamine from graphite and amorphous water ice surfaces," *Astron. Astrophys.* **612**, A47 (2018).

⁴⁸J.-H. Fillion, L. Amiaud, E. Congiu, F. Dulieu, A. Momeni, and J.-L. Lemaire, "D₂ desorption kinetics on amorphous solid water: From compact to porous ice films," *Phys. Chem. Chem. Phys.* **11**(21), 4396–4402 (2009).